Nanoscale

RSC Publishing

COMMUNICATION

Synthesis and characterization of p–n homojunction-containing zinc oxide nanowires†

Cite this: *Nanoscale*, 2013, **5**, 2259

Received 27th June 2012
Accepted 25th January 2013

DOI: 10.1039/c3nr31639d

www.rsc.org/nanoscale

Guohua Li,[a] Abhishek Sundararajan,[b] Anas Mouti,[ac] Yao-Jen Chang,[a] Andrew R. Lupini,[c] Stephen J. Pennycook,[cd] Douglas R. Strachan[b] and Beth S. Guiton*[ac]

We illustrate a simple method to synthesize highly ordered ZnO axial p–n homojunction-containing nanowires using a low temperature method, and on a variety of substrates. X-ray diffraction, scanning transmission electron microscopy, scanning electron microscopy, and Raman spectroscopy are used to reveal high quality single-crystalline wires with a [001] growth direction. The study of electrical transport through a single nanowire based device and cathodoluminescence *via* scanning transmission electron microscopy demonstrates that an axial p–n junction exists within each ZnO nanowire. This represents the first low temperature synthesis of axial p–n homojunction-containing ZnO nanowires with uniform and controllable diameters.

Introduction

Semiconductor nanowires serve as one of the most powerful platforms in nanoscience today due to their versatile structures and the ability to control composition from the atomic scale and up.[1–3] The design and synthetic realization of complex oxide nanowires with predictable physical properties is therefore of utmost importance for the advancement of both fundamental and applied research in this field.[4–8] Zinc oxide (ZnO) nanowires (NWs) have been heavily studied as promising alternatives to silicon, with reports including their use as building blocks for electronic–optoelectronic,[9,10] and energy harvesting/generating[11–13] applications. To date, rectifying devices made from these wires largely comprise heterojunctions between the wire and a substrate, rather than a homojunction geometry formed from the fabrication of a p–n junction contained within a single wire.

The p–n junction forms one of the basic elements of modern semiconductor devices.[14] As such, nanowires containing p–n junctions are a fundamental building block for a wide range of applications, such as photovoltaics. Thus far, a number of junction containing nanowire-based structural types have been investigated, with the major variations consisting of homo-*versus* hetero-junction materials, and axial *versus* radial junction geometries.[15–19] For example, Mueller *et al.*[14] and Lee *et al.*[20] used electrostatic doping to construct a single carbon nanotube-based axial p–n junction diode, and hetero-junctions with ZnO nanorods on different substrates were recently reported.[21,22] Core–shell nanowire structures generally forming radial p–n junctions have been explored extensively,[23–25] and axial p–n junctions have also been realized in Si nanowires by ion-implanation.[26] However, the synthesis of an axial p–n homojunction within a single nanowire using a facile technique is still rare. Pradhan *et al.*[27] reported a method to synthesize p–n junction-containing ZnO nanowires, yet the p–n junctions produced by this method were not strictly axial, since radial growth must also occur during the second step of the synthesis. In this communication, we illustrate a simple method to synthesize highly ordered ZnO axial p–n homojunction-containing nanowires with a low temperature synthesis, and on a variety of substrates. Detailed characterization of the as-synthesized wires reveals the existence of a single, axial, p–n homojunction within each nanowire.

Experimental details

Synthesis of ZnO p–n junction nanowire arrays

In this paper, we explore an aqueous *in situ* doping method to synthesize vertical ZnO nanowire arrays containing an axial p–n junction within each wire. The ZnO nanowire arrays are grown on several different substrates including: (001) silicon, c-sapphire, and ITO (indium-tin-oxide)-coated glass at temperatures below 100 °C in all cases.

The synthesis process is as follows: first, the substrate (silicon, c-sapphire, or ITO-coated glass) is cleaned by sonication

[a]*Department of Chemistry, University of Kentucky, Lexington, Kentucky 40506, USA. E-mail: beth.guiton@uky.edu*

[b]*Department of Physics and Astronomy, University of Kentucky, Lexington, Kentucky 40506, USA*

[c]*Materials Science and Technology Division, Oak Ridge National Laboratory, Oak Ridge, Tennessee 37831, USA*

[d]*Department of Materials Science and Engineering, University of Tennessee, Knoxville, Tennessee 37996, USA*

† Electronic supplementary information (ESI) available. See DOI: 10.1039/c3nr31639d

This journal is © The Royal Society of Chemistry 2013

in acetone, isopropyl alcohol (IPA), and deionized (DI) water consecutively, followed by treatment in an ultraviolet ozone (UVO) cleaner. The substrate is then spin coated with 5 mM zinc acetate solution in IPA followed by baking at 350 °C for 30 min in air, causing the zinc acetate particles formed by spin coating to thermally decompose to form zinc oxide (ZnO) nanocrystallite seeds for subsequent nanowire growth. The nanowire growth process consists of two steps: the growth of a p-type ZnO NW section (*via* Li-doping), followed by an intrinsic n-type section. p-type ZnO nanowire growth is achieved by heating the seeded substrate at 92 °C in 200 mL of growth solution comprising 5 mM zinc acetate dihydrate (99.99%, Alfa Aesar), 5 mM hexamethylenetetramine (HMTA, 99.9%, Alfa Aesar), 0.1 mM lithium chloride (99.9%, Alfa Aesar), and 3 mM polyethyleneimine (PEI, wt 600, 99.9%, Alfa Aesar) for 3 h. An (optional) n-type section is then grown axially by removing the substrate from solution, and placing it into an identical fresh solution – in this case containing no lithium chloride – again heating at 92 °C for 3 h. The as-synthesized ZnO nanowire p–n junction arrays are rinsed with IPA and DI water and finally annealed at 450 °C in air for 30 min to remove any residual organics.

Structural characterization and device fabrication

The as-synthesized ZnO nanowires were initially checked for phase purity and the correct structure using powder X-ray diffraction (XRD) with a D8 ADVANCE Bruker AXS (Cu Kα radiation) diffractometer. Raman spectra were obtained on a HORIBA (iHR320) Scientific Raman system combined with a 633 nm HeNe excitation laser (Thorlabs).

Structural characterization of individual wires was performed using a scanning electron microscope (Hitachi S-4300 SEM) operated at 30 kV, and a fifth-order aberration-corrected dedicated scanning transmission electron microscope (Nion UltraSTEM, Oak Ridge National Laboratory STEM Group) operated at 60 and 100 kV.

The nanowires were then analysed by STEM cathodoluminescence (STEM-CL) in a JEOL 2200FS (S)TEM equipped with a Gatan Xiclone MonoCL2 cathodoluminescence detector, at an acceleration energy of 80 keV. STEM-CL samples were prepared as standard TEM grids *via* sonication in and drop-casting from ethanol solution.

To fabricate p-type and p–n junction nanowire devices, the ZnO nanowires were dispersed on clean silicon substrates with 300 nm thermal oxide. Standard E-beam lithography (Raith E-Line) procedures were used to fabricate the two terminal devices, followed by e-beam evaporation of Ti/Au and lift-off.

Results and discussion

Our synthetic approach is shown schematically in Fig. 1. This synthesis combines aspects from the preparation of p–n junction containing ZnO wires first developed by Pradhan *et al.*,[27] with the additional use of polyethyleneimine (PEI) to inhibit radial and promote axial nanowire growth.[28,29] The use of PEI during the synthesis is therefore crucial for forming only axial p–n junctions within the ZnO nanowire.

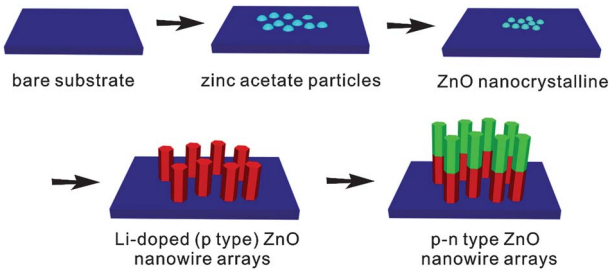

Fig. 1 Schematic diagram to show the synthesis of p–n junction-containing ZnO nanowire arrays.

The XRD data of as-grown samples on different substrates are shown in Fig. S1(a) of ESI.† Only one sharp peak at 34.5° is detected, corresponding to hexagonal wurtzite (002). This single, highly intense diffraction peak indicates that the as-grown ZnO NWs are highly crystalline, and suggests that they have a preferential growth direction of [001]. The Raman spectrum (Fig. S1(b) in ESI†) of the as-grown sample on an ITO substrate shows only one dominant peak centered at 436.9 cm^{-1}, which is attributed to ZnO E_2 (high) mode.

The morphology of the ZnO nanowire arrays was examined by field emission SEM. SEM images taken with a 40° tilt are

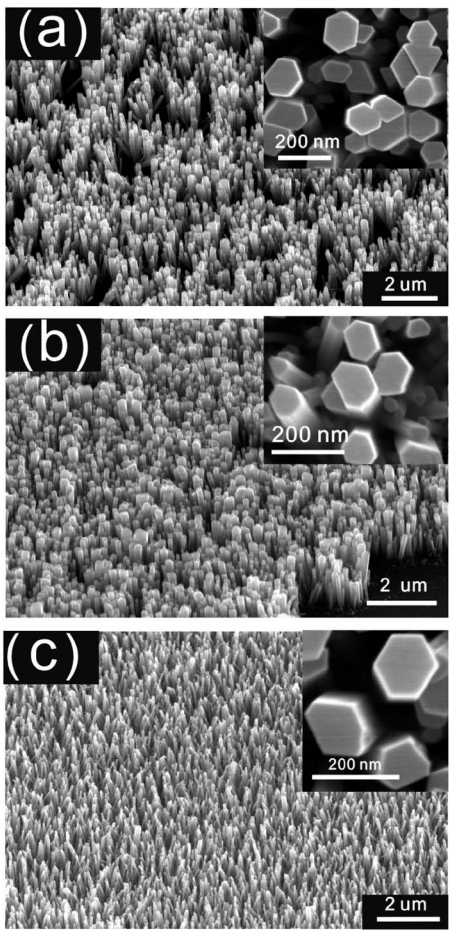

Fig. 2 SEM images of as-synthesized ZnO p–n junction nanowires on (a) ITO-coated glass, (b) c-sapphire, and (c) (001) silicon substrates. Insets: magnified images of the top view of the wires, showing the hexagonal nanowire cross-section.

This journal is © The Royal Society of Chemistry 2013

shown in Fig. 2(a)–(c), for the three different substrates investigated. These images show ZnO nanowire arrays which are highly aligned, growing vertically from the ITO-coated glass, sapphire, and silicon substrates, suggesting that our synthetic method is substrate-independent. The insets to Fig. 2(a)–(c) are a top view of the corresponding ZnO nanowire arrays taken with zero tilt, and show wires with hexagonal cross-sections in all cases. This shape is indicative of a wurtzite structure with [001] (*c*-axis) growth direction, consistent with XRD results discussed above. SEM images show the lengths and diameters of the ZnO nanowires to be in the 1–3 μm and 60–100 nm ranges, respectively. These dimensions were shown to be controllable with our reaction conditions, using reactant concentrations and the size of ZnO nanocrystalline seeds (*via* the thermal decomposition temperature of zinc acetate particles) to control wire diameter, and reaction time to control wire length. The obtained nanowire densities in our experiment are in the range of 5–80 μm^{-2}, which was sufficiently low to avoid mass-transport limited growth,[30,31] and to obtain linear dependence of nanowire length on the growth time. The low weight polyethyleneimine (PEI) was key to forming nanowires of constant diameter, since this molecule preferentially adsorbs to the bounding {1010} facets of the ZnO wires, inhibiting radial growth and therefore promoting axial growth of the nanowires at the beginning of the growth process.[28,29]

The structure of individual p–n junction-containing nanowires was further studied using scanning transmission electron microscopy (STEM). Fig. 3(a) and (b) show the single-crystalline structure of a typical ZnO nanowire. The spacing of the lattice fringes measured from Fig. 3(b) is ~0.52 nm, which corresponds to the (001) planes of wurtzite ZnO. The inset to Fig. 3(b) is a fast Fourier transform (FFT) of this area; indexing of the FFT infers a [001] growth direction. Fig. 3(c) shows the typical morphology of a single nanowire p–n junction with a length of 1.5 μm and a diameter of 70 nm. Remarkably, this Z-contrast annular dark field (ADF) image reveals dark pockets, mostly located on one side of the nanowire as shown in Fig. 3(d). Since darker regions indicate regions of lower atomic mass in ADF images, this identifies these dark spots as regions of high Li concentration. The wires and these Li pockets are stable under the e-beam, and indicate that doping – while mostly segregated to one side of each wire as desired, is not homogeneous. All of the wires investigated by STEM showed this feature.

The direct detection of Li-doping is challenging, since the ratio of Li to Zn in the initial solution is only about 2%, and moreover, lithium is the third lightest element, both factors which contribute to preventing its detection by energy

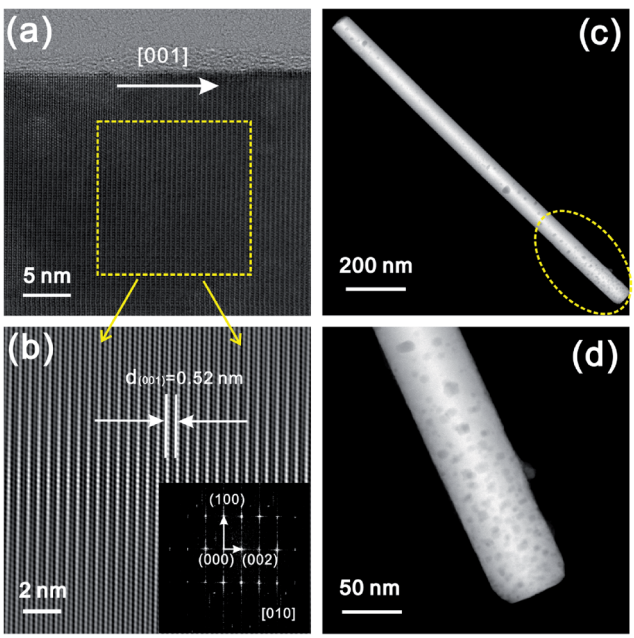

Fig. 3 STEM images of a typical ZnO p–n junction nanowire. (a) Bright field image, and (b) filtered section of the same image, showing the hexagonal crystal structure of the nanowire with [001] growth direction. Inset to (b): fast Fourier transform. (c) Annular dark field image of the same wire, and (d) magnified image of the circled part of (c), demonstrating pockets of Li-doping localized mostly on one side of the wire.

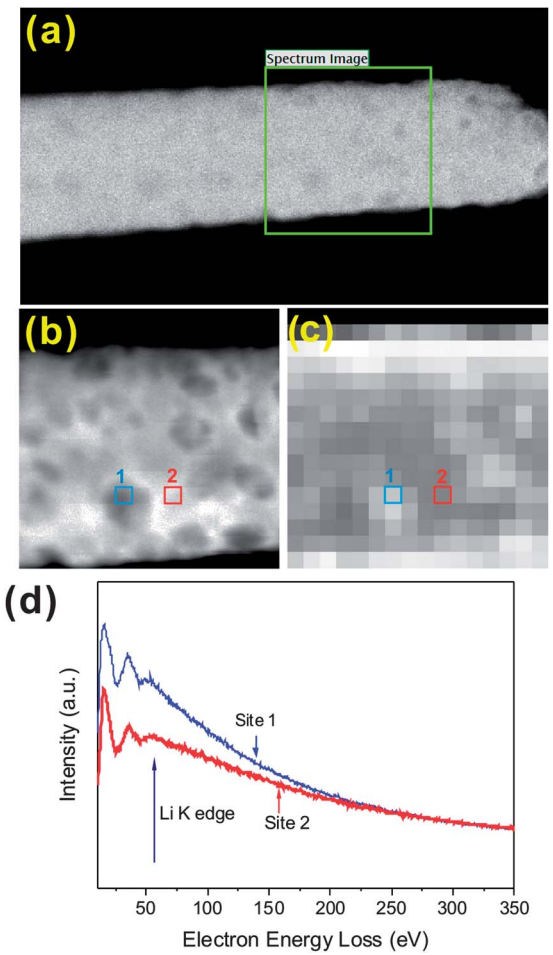

Fig. 4 EEL spectrum imaging of annealed p–n junction ZnO nanowires. (a) ADF image showing the region chosen for subsequent spectrum imaging. (b) ADF image and (c) an energy slice from a spectrum image taken simultaneously, both from the region indicated in (a). (d) Spectra from the sites labelled 1 and 2 in (b) and (c), showing the Li K edge at ~55 eV, with greater intensity from site 1, corresponding to a dark spot in the ADF image. The lower energy plasmon peaks are under current investigation.

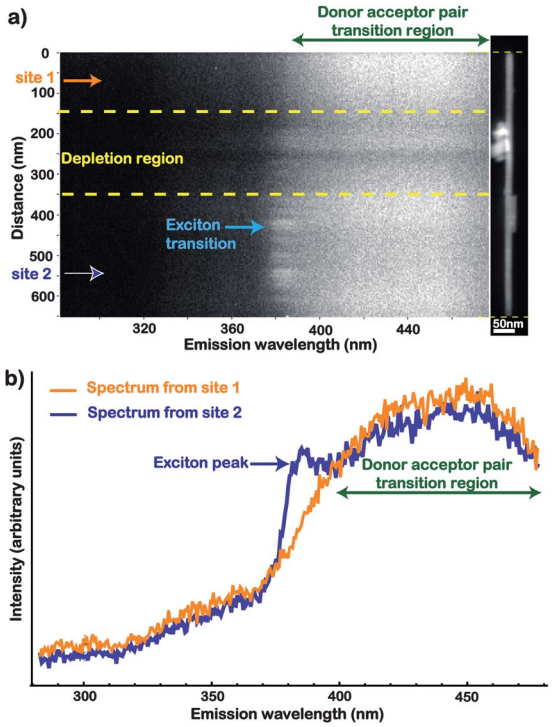

Fig. 5 Cathodoluminescence analysis of a single nanowire. (a) Line-scan spectrum image with corresponding annular dark field STEM image. A dip in emission is seen in the middle of the wire, while the two sides of the nanowire show different luminescence characteristics. (b) Two spectra from the upper part of the nanowire (site 1) and the lower part (site 2), showing a donor acceptor pair region on both sides of the junction, but an excitonic peak from only one side of the wire.

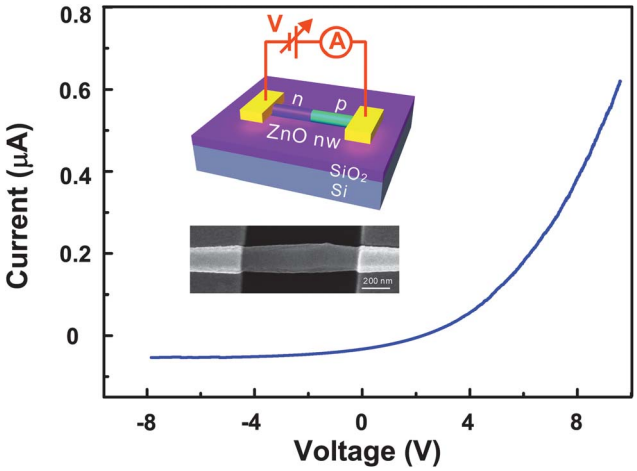

Fig. 6 Current–voltage characteristic of a two-terminal device based on a single ZnO p–n junction nanowire. Insets: schematic diagram (upper) and SEM image (lower) of the device.

dispersive X-ray spectroscopy. In order to detect the Li directly, therefore, we employed electron energy loss spectroscopy (EELS) spectrum imaging, to map the Li K edge (~55 eV) as a function of beam position in the STEM (Fig. 4). This data confirms that Li is contained within the wire, as demonstrated by the existence of the Li K edge in each of the spectra (pixels) contained within the spectrum image. The peak positions we measure are consistent with those recently reported by Hong's group.[32] Additionally, spectrum imaging allows us to compare the EELS spectra taken from darker regions of the Z-contrast image with those from lighter regions. We find that spectra collected from the darker regions have higher Li K edge intensities than those taken from brighter regions, consistent with our hypothesis that the darker regions contain greater concentrations of Li. Accordingly, the Z-contrast image itself may be taken as indirect evidence of (inhomogeneous) Li-doping, where dark spots in the image demonstrate a region of successful Li-doping.

To verify the existence of an axial p–n junction within each ZnO nanowire, we performed cathodoluminescence measurements upon individual nanowires. Fig. 5 shows the cathodoluminescence analysis of a nanowire, confirming the existence of a single axial p–n junction within the wire. Fig. 5(a) features a line-scan spectrum image aligned with its corresponding dark STEM image. A dip in emission is noticed in the middle of the nanowire, while the two sides of the nanowire show different luminescence characteristics. On the upper side of the emission dip only the donor–acceptor pair (DAP) band, and no excitonic peak, was detected. On the lower side, however, an excitonic peak could be resolved, even though the DAP band is still present. The asymmetry of exciton emission is evidence of an asymmetric dopant distribution. The presence of a dip in emission between the two sides of the wire further confirms the dopant asymmetry, and is therefore identified as the depletion layer. Fig. 5(b) compares two spectra from the upper part of the nanowire (site 1) and the lower part (site 2), showing clearly the difference in emission between the two parts.

Since rectifying behaviour is an essential property of the p–n junction, the current–voltage characteristic of the nanowires was measured from electron-beam lithographically fabricated nanodevices (Fig. 6). The insets to Fig. 6 show a schematic diagram of a two terminal device, and a SEM image of the device. The channel gap is ~1 μm, and the diameter of the ZnO NW is ~200 nm. The current–voltage characteristic from this device shows obvious asymmetric rectifying behaviour, which is consistent with the presence of a p–n homojunction within the nanowire. For comparison, we also measured the *I–V* characteristics of pure p-type wires, in which only the Li-doped section was grown during synthesis. In contrast to the electrical behaviour of the nanowires doped on only one side, these pure p-type wires showed symmetric *I–V* characteristics (Fig. S2†). To verify that the Li-doped region of our wires is indeed p-type we measured these same devices as a function of gate voltage, demonstrating that the conductance increases under negative V_g and decreases with positive applied V_g (Fig. S3†).

Conclusions

In conclusion, we have developed a low temperature and facile method to synthesize highly ordered ZnO axial p–n junction-containing nanowires on different substrates. This demonstrates the first example of a low temperature solution-phase synthesis of a p–n homojunction containing nanowire *via* selective *in situ* lithium (p-type) doping of one side of each nanowire. Structural

 This journal is © The Royal Society of Chemistry 2013

characterization reveals high quality single-crystalline wires with a [001] unique growth direction, and cathodoluminescence and current–voltage measurements demonstrate that an axial p–n junction exists within each ZnO nanowire.

Acknowledgements

Many thanks to Prof. P Stadelmann, Prof. C. Hebert and the CIME laboratory (École Polytechnique Fédérale de Lausanne) for allowing us the use of their JEOL 2200FS STEM with CL detector. This research was supported by Oak Ridge National Laboratory's Laboratory Directed Research and Development Fund (AM, BSG), the Office of Basic Energy Sciences, Materials Sciences and Engineering Division, U.S. Department of Energy (SJP, ARL), and partially supported by the Kentucky NSF EPSCoR program through the Center of Advanced Materials (GL, DRS, BSG).

Notes and references

1 C. M. Lieber, *MRS Bull.*, 2011, **36**, 1052–1063.
2 T. Y. Zhai, L. Li, Y. Ma, M. Y. Liao, X. Wang, X. S. Fang, J. N. Yao, Y. Bando and D. Golberg, *Chem. Soc. Rev.*, 2011, **40**, 2986–3004.
3 T. Y. Zhai, X. S. Fang, L. Li, Y. Bando and D. Golberg, *Nanoscale*, 2010, **2**, 168–187.
4 K. W. Wu, H. P. He, Y. F. Lu, J. Y. Huang and Z. Z. Ye, *Nanoscale*, 2012, **4**, 1701–1706.
5 H. J. Fan, Y. Yang and M. Zacharias, *J. Mater. Chem.*, 2009, **19**, 885–900.
6 J. Cao, E. Ertekin, V. Srinivasan, W. Fan, S. Huang, H. Zheng, J. W. L. Yim, D. R. Khanal, D. F. Ogletree, J. C. Grossmanan and J. Wu, *Nat. Nanotechnol.*, 2009, **4**, 732–737.
7 C. W. Cheng, B. Liu, H. Y. Yang, W. W. Zhou, L. Sun, R. Chen, S. F. Yu, J. X. Zhang, H. Gong, H. D. Sun and H. J. Fan, *ACS Nano*, 2009, **3**, 3069–3076.
8 J. Cho, Q. B. Lin, S. Yang, J. G. Simmons, Y. W. Cheng, E. Lin, J. Q. Yang, J. V. Foreman, H. O. Everitt, W. T. Yang, J. Kim and J. Liu, *Nano Res.*, 2012, **5**, 20–26.
9 P. C. Chang and J. G. Lu, *IEEE Trans. Electron Devices*, 2008, **55**, 2977–2987.
10 L. Li, G. Meng, H. Q. Wang, T. Y. Zhai, X. S. Fang, U. K. Gautam, X. D. Fang, Y. Bando and D. Golberg, *Chem. Commun.*, 2011, **47**, 8247–8249.
11 S. Dunn, J. Briscoe, D. E. Gallardo, S. Hatch, V. Lesnyak and N. Gaponik, *J. Mater. Chem.*, 2011, **21**, 2517–2523.
12 Z. L. Wang and J. H. Song, *Science*, 2006, **312**, 242–246.
13 C. Xu and Z. L. Wang, *Adv. Mater.*, 2011, **23**, 873–877.
14 T. Mueller, M. Kinoshita, M. Steiner, V. Perebeinos, A. A. Bol, D. B. Farmer and P. Avouris, *Nat. Nanotechnol.*, 2010, **5**, 27–31.
15 C. Y. Wen, M. C. Reuter, J. Bruley, J. Tersoff, S. Kodambaka, E. A. Stach and F. M. Ross, *Science*, 2009, **326**, 1247–1250.
16 T. E. Clark, P. Nimmatoori, K. K. Lew, L. Pan, J. M. Redwing and E. C. Dickey, *Nano Lett.*, 2008, **8**, 1246–1252.
17 D. E. Perea, N. Li, R. M. Dickerson, A. Misra and S. T. Picraux, *Nano Lett.*, 2011, **11**, 3117–3122.
18 J. Gao, O. I. Lebedev, S. Turner, Y. F. Li, Y. H. Lu, Y. P. Feng, P. Boullay, W. Prellier, G. van Tendeloo and T. Wu, *Nano Lett.*, 2012, **12**, 275–280.
19 M. Paladugu, J. Zou, Y. N. Guo, G. J. Auchterlonie, H. J. Joyce, Q. Gao, H. H. Tan, C. Jagadish and Y. Kim, *Small*, 2007, **3**, 1873–1877.
20 J. U. Lee, P. P. Gipp and C. M. Heller, *Appl. Phys. Lett.*, 2004, **85**, 145–147.
21 B. Nikoobakht and A. Herzing, *ACS Nano*, 2010, **4**, 5877–5886.
22 T. I. Lee, S. H. Lee, Y. D. Kim, W. S. Jang, J. Y. Oh, H. K. Baik, C. Stampfl, A. Soon and J. M. Myoung, *Nano Lett.*, 2012, **12**, 68–76.
23 B. Z. Tian, X. L. Zheng, T. J. Kempa, Y. Fang, N. F. Yu, G. H. Yu, J. L. Huang and C. M. Lieber, *Nature*, 2007, **449**, U885–U888.
24 J. Y. Tang, Z. Y. Huo, S. Brittman, H. W. Gao and P. D. Yang, *Nat. Nanotechnol.*, 2011, **6**, 568–572.
25 O. Hayden, A. B. Greytak and D. C. Bell, *Adv. Mater.*, 2005, **17**, 701–704.
26 S. Hoffmann, J. Bauer, C. Ronning, T. Stelzner, J. Michler, C. Ballif, V. Sivakov and S. H. Christiansen, *Nano Lett.*, 2009, **9**, 1341–1344.
27 B. Pradhan, S. K. Batabyal and A. J. Pal, *Appl. Phys. Lett.*, 2006, **89**, 233109.
28 M. Law, L. E. Greene, J. C. Johnson, R. Saykally and P. D. Yang, *Nat. Mater.*, 2005, **4**, 455–459.
29 L. E. Greene, B. D. Yuhas, M. Law, D. Zitoun and P. D. Yang, *Inorg. Chem.*, 2006, **45**, 7535–7543.
30 J. E. Boercker, J. B. Schmidt and E. S. Aydil, *Cryst. Growth Des.*, 2009, **9**, 2783–2789.
31 G. P. Li, L. Jiang, S. J. Wang, X. W. Sun, X. D. Chen and T. Wu, *Cryst. Growth Des.*, 2011, **11**, 4885–4891.
32 J. Lee, S. Cha, J. Kim, H. Nam, S. Lee, W. Ko, K. L. Wang, J. Park and J. Hong, *Adv. Mater.*, 2011, **23**, 4183.

This journal is © The Royal Society of Chemistry 2013